RESEARCH ARTICLE

A Novel Control Approach for a Single-Inductor Multi-Input Single-Output DC–DC Boost Converter for PV Applications

ALIREZA ASADI[1], **MOHAMMAD SALEH KARIMZADEH**[2],
XIAODONG LIANG[1], **(Senior Member, IEEE), MOHAMMAD SAEED MAHDAVI**[2],
AND GEVORK B. GHAREHPETIAN[2], **(Senior Member, IEEE)**
[1]Department of Electrical and Computer Engineering, University of Saskatchewan, Saskatoon, SK S7N 5A9, Canada
[2]Department of Electrical Engineering, Amirkabir University of Technology (Tehran Polytechnic), Tehran 15916-34311, Iran

Corresponding author: Xiaodong Liang (xil659@mail.usask.ca)

ABSTRACT In this paper, a single-inductor multi-input single-output (SI-MISO) DC-DC boost converter is used for solar photovoltaic (PV) systems in DC or AC grids. The converter with N number of inputs combines energy from PV panels along with fuel cells (FCs) to maintain stability. By implementing a new switching algorithm in the converter, the output voltage of the converter and the power absorbed from each source can be controlled independently, resulting in a simple and unique controller. In addition, the multivariable control system can be controlled as N number of single-input single-output (SISO) systems without any delay between switches due to the small-signal model of the converter and the proposed proportional-integral-derivative (PID) cascade control scheme. For each PV source, an independent maximum power point tracking (MPPT) algorithm can be employed, and the current sharing among different sources can be achieved independently. The converter's operating modes and the designed controller are present in the paper. Experimental results using a 100-W prototype converter validate the accuracy and efficiency of the proposed control scheme.

INDEX TERMS Multi-input single-output dc–dc converter, photovoltaic systems, proportional-integral-derivative (PID) cascade control, renewable energy.

I. INTRODUCTION

Renewable energy sources, such as solar photovoltaic (PV) systems, are increasingly integrated into our modern power grids. However, variables, including sun exposure, temperature, and shadow fluctuations, have significant impacts on the efficiency of PV panels [1]. It is essential to combine multiple energy sources (PV panels, wind turbines, fuel cells, or batteries) in an energy conversion system due to their mutually complementary nature [2], [3]. The integrated power supply system is more flexible, reliable, and efficient than conventional single-PV sources with the maximum power point tracking (MPPT). A typical procedure to convert energy

The associate editor coordinating the review of this manuscript and approving it for publication was Yang Tang.

from multiple sources is to link two or more DC voltage sources to DC-DC converters and create a steady output voltage for the load with a proper control setup [4], [5]. The use of multiple independent single-input, single-output (SISO) DC-DC converters provides some advantages, such as being user-friendly, but also requires a large number of components and a high cost. To address these problems, References [3], [6], and [7] have proposed various types of multi-input, multi-output DC-DC converters, in which the quantity of semiconductors and inductors is effectively reduced, and thus, enhance the power density and reduce the price. A PV system, along with batteries, supercapacitors, or fuel cells (FCs), can be integrated through a multi-input DC-DC converter [8], as shown in Fig. 1, forming a hybrid energy grid-tied system.

A multi-input converter can be categorized into two major categories: isolated and non-isolated. Isolated DC-DC converters are suitable for applications that require isolation between inputs and outputs. Using a multi-winding transformer for electrical isolation in an isolated multi-input converter increases the size and the total losses. In [9], [10], and [11], different types of isolated converters are introduced. On the other hand, it is possible to design a PV system with a less complex structure and enhance its efficiency by using non-isolated multi-input DC-DC converters [12], [13]. In this paper, the non-isolated single-inductor multi-input single-output (SI-MISO) DC-DC converter introduced in [7] (Fig. 2) is adopted.
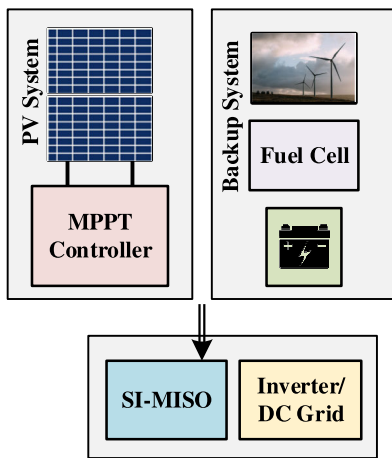

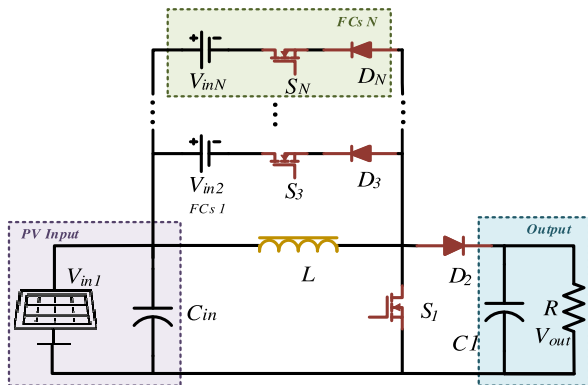**FIGURE 1.** Hybrid energy grid-tied systems.

FIGURE 2. The non-isolated SI-MISO DC-DC converter [7].

The SI-MISO DC-DC converter only has one inductor, and the inductor is the only path for power to flow through all ports, thereby achieving high power density and reducing the overall volume and weight of the converter [14]. Current sharing while simultaneously regulating the output voltage is one of the main challenges in the design of multi-input converters. Variations in each input source can also affect the control of other input sources. For instance, FCs have become increasingly popular as auxiliary power sources due to their cleanliness, high efficiency, and stable performance.

However, the long startup period and slow transient characteristics of FCs make them hard to combine with other sources [1], [12]. To achieve the MPPT, current sharing between input sources, output voltage regulation, and the total absorbed power control simultaneously, an effective multivariable control system is urgently needed.

Although non-isolated multi-input converters have a lower cost, smaller size and higher efficiency, controlling these converters has always been a challenge, specifically when the converter is used in PV applications and the MPPT is required for PV inputs. From the control perspective, multi-input converters are multivariable systems, and their control is different from SISO converters. Many linear and non-linear methods are available to control multi-input converters, each with advantages and disadvantages. In [1], [14], and [15], a decoupling network is introduced to change a multi-variable/input system into multiple SISO systems, but the MPPT cannot be used, and a system with a high number of inputs becomes very complicated and unstable. Other methods to control MIMO converters are proposed in [16] and [17], but they are complicated, and also do not have the MPPT.

To overcome these challenges, in this paper, we propose an effective control method for the SI-MISO DC-DC converter for PV applications. The main contributions of this paper include:

1) Using the proposed control method, each PV source is equipped with a MPPT control, and the whole system has an output voltage controller, all working independently. This proposed control method is applicable to all multi-port DC-DC converters with similar switching behavior as the studied SI-MISO DC-DC converter.

2) Generally, the output voltage of a boost converter cannot be controlled directly by linear controllers. In this paper, a proportional-integral-derivative (PID) cascade controller is proposed to control the output voltage of the converter indirectly through the inductor current [4], [18], [19].

3) The proposed PID cascade controller is simple to implement, and has high robustness and fast dynamics, which has been proven through experimental results in Section V.

The paper is organized as follows: in Section II, the SI-MISO converter is introduced; the novel control method is proposed in Section III; in Section IV, experimental results using a 100 W prototype are provided to validate the proposed control performance in the SI-MIMO converter; and conclusions are drawn in Section V.

II. CONVERTER ANALYSIS AND DESIGN

The SI-MISO converter used in this study is shown in Fig. 2. There are multiple input power sources, a PV system (V_{in1}) and (N-1) FCs (V_{in2})-(V_{inN}) to provide a reliable output. R is the load resistance, representing the equivalent power supplied by a grid-connected inverter. There are power switches, S_1, S_3, …., S_N, that control the output voltage and power flow of the converter. Based on the number of input sources,

working restrictions are applied to the circuit; and to simply the circuit, the branch with unidirectional switches, MOS-FETs and diodes is converted into a single diode (S_1) and a MOSFET (D_2); otherwise, we can add D_1 in S_1 branch and S_2 in D_2 branch to rectify the restrictions [14].

To simplify the operating mode analysis, the dual-input version (*one PV and one FC*) of the converter is evaluated. The following are restrictions of the converter with two inputs:

1) $V_{in1} > V_{in2}$
2) $V_{out} > V_{in1}$

Figs. 3 and 4 show operating modes and waveforms, respectively. To simplify the converter analysis, it is assumed that the semiconductor devices are ideal, the voltage of all capacitors is constant, and the magnetizing inductance L is large enough, leading to a constant inductor current (I_L) with low current ripples. Working conditions are determined by polarities of the switches. When using more than two input sources, the same analysis method applies, and all switches in branches parallel to the inductor behave exactly like the switch S_3. Working restrictions are rectified by the proposed output voltage controller, which has a high stability around the operating point of the converter.

A. VOLTAGE GAIN AND COMPONENTS DESIGN

In the SI-MISO converter, the inductor is energized at the first two working stages, and de-energized at the last working stage to supply the load. Therefore, the switching period of the converter has three different operating modes based on the switches and one inductor as follows:

Interval 1 ($t_0 \sim t_1$) [Fig. 3(b)]: In this mode, from the beginning of this interval (t_0), the gate-source signal to both switches is applied, and only the switch S_1 conducts. The energy of the first input source *(PV)* is transferred to the inductor and the inductor voltage is V_{i_1}. The capacitor, C_1, is discharging, and the capacitor, C_{in}, is transferring energy to the inductor. The diodes, D_3 and D_2, and the switch, S_3, are reverse biased and do not conduct. The following equations are derived based on Kirchhoff's current law *(KCL)*:

$$V_L = V_{i_1} = V_{C_{in}}, \quad i_{C_1} = -i_o, \quad i_{C_{in}} = i_{in_1} - i_L \quad (1)$$
$$V_{D_2} = -V_o < 0, \quad V_{DS_3} = V_{i_2} - V_{i_1} < 0 \quad (2)$$

where Eq. (2) shows why D_3, D_2 and S_3 are reverse biased.

Interval 2 ($t_1 \sim t_2$) [Fig. 3(c)]: At t_1, the gate-source signal of the switch, S_1, is turned off, while the gate-source signal of S_3 is still applying. In this mode, the switch, S_3, conducts. This time, the energy of the second input source *FC* is transferred to the inductor and is being charged by the voltage of V_{i_2}. Moreover, the capacitor, C_1, is discharging, while the capacitor, C_{in}, is charging from the first input. The diode, D_1, is reverse biased and does not conduct, and the switch, S_1, is turned off. The following equations are derived based on

Kirchhoff's current law *(KCL)*:

$$V_L = V_{i_2}, \quad V_{i_1} = V_{C_{in}}, \quad i_{C_1} = -i_o, \quad i_{C_{in}} = i_{in_1} \quad (3)$$
$$V_{S_1} = V_{i_1} - V_{i_2} > 0, \quad V_{D_2} = V_{i_1} - (V_{i_2} + V_o) < 0 \quad (4)$$

Interval 3 ($t_2 \sim t_3$) [Fig. 3(d)]: At t_2, both switches, S_1 and S_3, are turned off. Only the diode D_2 is conducting. The energy from the inductor and the first input is transferred to the load, and the inductor is being discharged by the voltage of $V_i - V_o$. The capacitor C_1 is charging, while the capacitor C_{in} is discharging. In this mode, the diode D_3 is turned off. The following equations are derived:

$$V_L = V_{i_1} - V_o, \quad i_{C_1} = i_L - i_o, \quad i_{C_{in}} = i_{in_1} - i_L \quad (5)$$
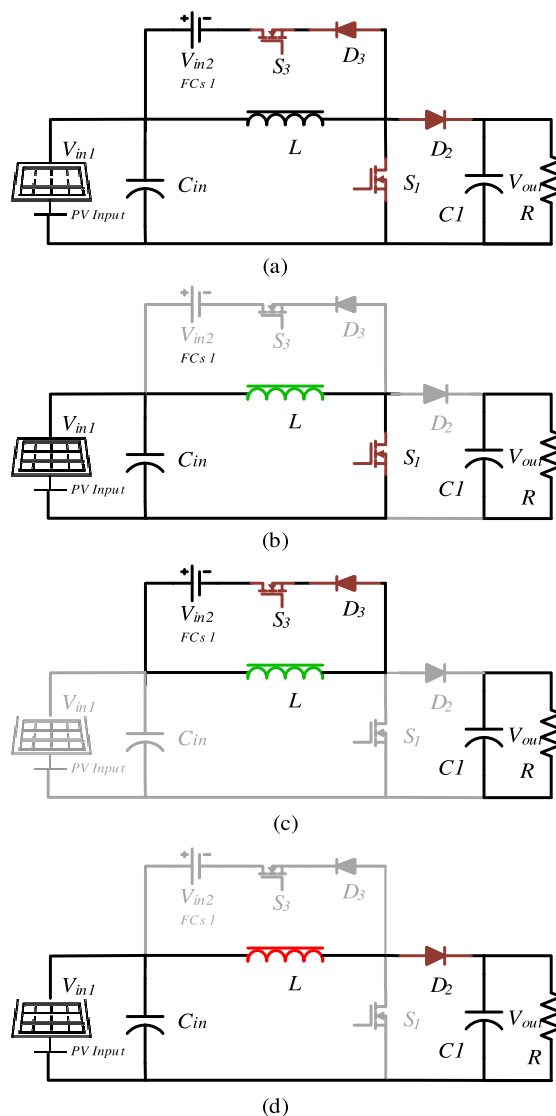$$V_{S_1} = V_o + V_{i_2} - V_{i_1} > 0, \quad V_{DS_3} = V_o > 0 \quad (6)$$

FIGURE 3. The SI-MISO converter and its equivalent circuits in different working stages: (a) converter, (b) [t_0, t_1] in CCM, (c) [t_1, t_2] in CCM, (d) [t_2, t_3] in CCM.

By applying the flux balance theory to the inductor, the following equations are derived from (1), (3) and (5) to

calculate the inductor current in (7). The voltage relationship between V_o, V_{i_1} and V_{i_2} is shown in (8).

$$i_L = \frac{i_o}{D_2} = \frac{V_o}{R_1 \times D_2}, \quad i_L = \frac{i_2}{D_3}, \quad i_L = \frac{i_1}{D_1 + D_2} \quad (7)$$

$$V_o = \frac{(D_1 + D_2) \times V_{i_1} + D_3 \times V_{i_2}}{D_2} \quad (8)$$
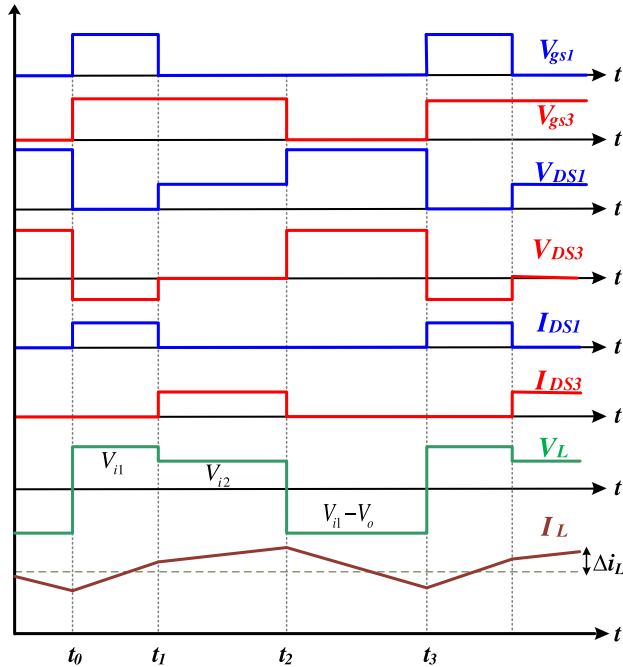

FIGURE 4. Waveforms of the switches gate signals (V_{gs_1} and V_{gs_3}), drain-source voltages (V_{DS_1} and V_{DS_3}) and currents (I_{DS_1} and I_{DS_3}), and the inductor voltage (V_L) and current (I_L) of the studied converter under steady state.

By considering a desired peak-to-peak ripple current, the inductance of the inductor in the circuit is determined in (9). The converter is designed to work in the continuous-conduction mode (CCM), thereby, the inductor current will never be zero. Based on this working condition, the minimum inductor capacity can be obtained in (10).

$$L = \frac{(V_{i_1} - V_o) \times D_2}{2 \times \Delta i_L} \times T_S$$
$$= \frac{V_{i_2} \times D_3 + V_{i_1} \times D_1}{2 \times \Delta i_L} \times T_S \quad (9)$$

$$L_{Min}$$
$$= Min \left\{ \begin{array}{c} D_2^2 \times \left[(V_o - V_{i_1}) \left(\frac{R}{2 \times V_o} \right) \right] \times T_S \\ \frac{(R \times D_3 \times D_2 \times V_{i_2}) + (R \times D_1 \times D_2 \times V_{i_1})}{2 \times V_o} \times T_S \end{array} \right\} \quad (10)$$

The peak-to-peak ripple voltage is used to determine the capacitance of the capacitors C_1 and C_{in} as follows:

$$C_1 = \frac{(1 - D_2) \times i_o}{2 \times \Delta V_{C_1}} \times T_S = \frac{(D_1 + D_3) \times i_o}{2 \times \Delta V_{C_1}} \times T_S \quad (11)$$

$$C_{in} = \frac{(D_1 + D_3) \times i_{i_1}}{2 \times \Delta V_{C_1}} \times T_S \quad (12)$$

B. DYNAMIC MODELING OF THE CONVERTER

The multi-input converter is controlled by the switches, S_1, S_3, S_4, ..., and S_n. Each switch has a unique duty cycle. The output voltage and MPPT for the PV input can be adjusted through a proper switch duty cycle regulation. To design closed-loop controllers and study transient and steady state behaviors, the dynamic model of the SI-MISO converter must be obtained first. Small-signal configurations are necessary to describe the stability and transient behaviors of the converter.

An optimized controller is designed based on a small-signal model. In particular, for a MISO converter, an effective small-signal configuration is crucial for the closed-loop control and converter dynamics optimization. Unlike conventional single-input converters, a multiport converter is a high-order system, the symbolic derivation of its plant transfer function is rather monotonous, and it is challenging to find poles and zeros. Alternatively, the plant dynamics can be described in a matrix format, so the bode graph of different transfer functions can be plotted [20], [21]. Based on the small-signal modeling method [Y], the state variable, duty ratios, and input voltages include two parts, DC values (X, D, V) and perturbations $(\hat{x}, \hat{d}, \hat{v})$. The perturbations are assumed to be small during one switching cycle, and do not vary significantly over time. We have the following equations for the converter under study:

$$\begin{cases} i_L(t) = I_L + \hat{i}_L(t) \\ v_o(t) = V_o + \hat{v}_o(t) \\ d_1(t) = D_1 + \hat{d}_1(t) \\ d_3(t) = D_3 + \hat{d}_3(t) \\ \quad \vdots \\ d_n(t) = D_{n+1} + \hat{d}_{n+1}(t) \\ v_{pv}(t) = V_{pv} + \hat{v}_{pv}(t) \end{cases} \quad (13)$$

where $i_L(t)$ is the inductor current and $v_o(t)$ is the output capacitor voltage state variable. For a converter with more than one input, n is the number of switches in the MISO converter. In a three inputs model, for instance, n is equal to 3, and the duty cycle variables are $d_1(t)$, $d_3(t)$, and $d_4(t)$.

In this paper, there is only one PV source as the primary source, and other inputs parallel to the inductor aim to enhance the circuit reliability. Based on the equation of each variable, the inductor and capacitor equations are determined for each interval. The open-loop steady state equations of the converter are derived in (14), as shown at the bottom of the next page, for any number of inputs.

As a result of (15), as shown at the bottom of the next page, the system can be represented as a matrix using a state-space model, where x, y, and z are state variables. The state-space model is presented as follows:

$$\dot{\tilde{x}} = A\tilde{x} + B\tilde{u}$$
$$\tilde{y} = C\tilde{x} + D\tilde{u} \quad (16)$$

where $\tilde{u}$ is a vector of control variables contains control inputs, $d_1(t)$, $d_3(t)$, …, and $d_n(t)$, $\tilde{y}$ is a matrix of the system's outputs, and $\tilde{x}$ is a vector representing the state variables.

So, the matrixes $\dot{\tilde{x}}$, $\tilde{y}$, and $\tilde{u}$ are in the following form:

$$\dot{\tilde{x}} = \begin{bmatrix} \hat{i}_L(t) \\ \hat{v}_{pv}(t) \\ \hat{v}_o(t) \end{bmatrix}, \quad \tilde{y} = \begin{bmatrix} \hat{i}_L(t) \\ \hat{v}_o(t) \end{bmatrix}, \quad \tilde{u} = \begin{bmatrix} \hat{d}_1(t) \\ \hat{d}_3(t) \\ \vdots \\ \hat{d}_n(t) \end{bmatrix} \quad (17)$$

As a result of using the state equations (15), for the converter with a PV source and a backup FC source, the state space equations and A, B, C, and D matrices are as follows (18)–(20), as shown at the bottom of the next page.

C. INDEPENDENT CONTROL OF OUTPUT VOLTAGE AND INPUT POWER

There is an independent control of the input voltage and output voltage in the converter [12].

Firstly, according to (8), the terms $(D_1 + D_2)$ can be rewritten as $(1 - D_3)$, as we assume the whole cycle is equal to 1 ($D_1 + D_2 + D_3 = 1$). Also, $(1 - D_3 - D_1)$ is used to represent D_2. The output voltage equation of the converter is given by

$$V_o = \frac{(1 - D_3) \times V_{i_1} + D_3 \times V_{i_2}}{1 - D_3 - D1}, \quad D_3 > D_1 \quad (21)$$

According to (21), the output voltage is controlled only by D_3. The duty cycle of the switch connected to the input with
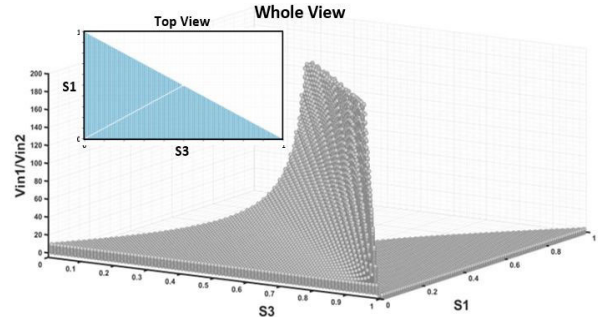

FIGURE 5. Relation of the two input voltages in the two-port SI-MISO converter to determine the main input.

the lowest voltage, known as the "main input" (S_3), is always higher than the duty cycle of switches connected to other inputs.

Fig. 5 shows that the duty cycle of switch S_3 is greater than the duty cycle of switch S_1. Other switches are slaves (S_1) if they are connected to a PV source with the MPPT. If it is assumed that ($D_3 > D_1$), we can estimate the denominator of (21) as $(1 - D_3)$. Therefore, the output voltage depends only on the main input. Fig. 5 illustrates (21) using MATLAB. In the region in blue color in Fig. 5 (top view), the duty cycle of S_3 (D_3) is higher than the duty cycle of S_1 (D_1), and it is always the case that V_{in1} is lower than V_{in2} in Fig. 5 (whole View), and the restrictions have been described in Section II. Fig. 5 indicates that, based on (21), the switch connected to the input with the lowest voltage (the main input) has a higher duty cycle than switches connected to other inputs.

$$Interval(1): L\frac{d\hat{i}_L(t)}{dt} = -\hat{v}_{pv}(t), \quad C_o\frac{d\hat{v}_o(t)}{dt} = -\frac{\hat{v}_o(t)}{R_o}, \quad C_{pv}\frac{dv_{pv}}{dt} = \frac{\hat{v}_{pv}(t)}{R_{pv_{eq}}} - \hat{i}_L(t)$$

$$Interval(2): L\frac{d\hat{i}_L(t)}{dt} = -V_{i_2}, \quad C_o\frac{d\hat{v}_o(t)}{dt} = -\frac{\hat{v}_o(t)}{R_o}, \quad C_{pv}\frac{d\hat{v}_{pv}(t)}{dt} = \frac{\hat{v}_{pv}(t)}{R_{pv_{eq}}}$$

$$Interval(3): L\frac{d\hat{i}_L(t)}{dt} = -V_{i_3}, \quad C_o\frac{d\hat{v}_o(t)}{dt} = -\frac{\hat{v}_o(t)}{R_o}, \quad C_{pv}\frac{d\hat{v}_{pv}(t)}{dt} = \frac{\hat{v}_{pv}(t)}{R_{pv_{eq}}}$$

$$\vdots \qquad\qquad\qquad \vdots \qquad\qquad\qquad\qquad (14)$$

$$Interval(n): L\frac{d\hat{i}_L(t)}{dt} = -V_{i_n}, \quad C_o\frac{d\hat{v}_o(t)}{dt} = -\frac{\hat{v}_o(t)}{R_o}, \quad C_{pv}\frac{d\hat{v}_{pv}(t)}{dt} = \frac{\hat{v}_{pv}(t)}{R_{pv_{eq}}}$$

$$Interval(n+1): L\frac{d\hat{i}_L(t)}{dt} = \hat{v}_{pv}(t) - \frac{\hat{v}_o(t)}{R_o}, \quad C_o\frac{d\hat{v}_o(t)}{dt} = \hat{i}_L(t) - \frac{\hat{v}_o(t)}{R_o}, \quad C_{pv}\frac{d\hat{v}_{pv}(t)}{dt} = \frac{\hat{v}_{pv}(t)}{R_{pv_{eq}}} - \hat{i}_L(t)$$

$$L\frac{d\hat{i}_L(t)}{dt} = \left(1 - \hat{d}_n(t)\right)\hat{v}_o(t) + \left(1 + \hat{d}_1(t) - \hat{d}_3(t) - \cdots - \hat{d}_n(t)\right)\hat{v}_{pv}(t)$$
$$+ \left(\hat{d}_3(t) + \cdots \hat{d}_n(t)\right)\left(-\hat{v}_o(t) - \hat{v}_{pv}(t) + V_{i_2} + \cdots + V_{i_n}\right) + \hat{d}_1(t)\left(\hat{v}_{pv}(t) - V_{i_2} - \cdots - V_{i_n}\right)$$

$$C_o\frac{d\hat{v}_o(t)}{dt} = \hat{i}_L(t)\left(1 - \hat{d}_n(t)\right) - \hat{i}_L(t)\left(\hat{d}_n(t)\right) - \frac{\hat{v}_o(t)}{R_o}$$

$$C_{pv}\frac{dv_{pv}(t)}{dt} = \frac{\hat{v}_{pv}(t)}{R_{pv_{eq}}} + \hat{i}_L(t)\left(2\hat{d}_n(t) + \cdots + 2\hat{d}_3(t) - 2\hat{d}_1(t) - 1\right) \quad (15)$$

Secondly, from (21), the output voltage V_o only depends on D_3, i.e., D_3 can solely control the output voltage of the converter. From (19), V_{pv} is related to both D_1 and D_3. Therefore, to design the MPPT, we can assume D_3 as a constant value corresponding to V_o. The MPPT is developed for the duty cycle of switch $S_1(D_1)$, and changes in D_3 are treated as disturbances, and the MPPT's PID controller adjusts D_1 in response to disturbances.

III. THE PROPOSED CONTROL SCHEME

Two major challenges in implementing multi-input converters are the current sharing and output voltage regulation. Variations of each input source affect the control of other input sources. Besides the duty cycle of switches needs to be controlled, the delay between switches should also be controlled for the MPPT and current sharing. Therefore, the current sharing and the MPPT algorithms of multi-input DC-DC converters are affected by various variables, which make their control circuit complicated.

For the SI-MISO converter in this paper, the MPPT control for each PV input source and the output voltage regulation are independent of each other, as explained in Section II. For the converter's control circuit design, the following two possibilities are considered [12]:

1) **Possibility 1**: To independently manage the output voltage in stand-alone applications, the voltage of at least one input source must be lower than the MPP voltage of PV cells. This source does not require the MPPT, and it can be fuel cells or backup batteries (Fig. 6).

2) **Possibility 2**: If PV cells are the only input sources, the MPPT is required, and all switches are regulated independently by the MPPT algorithms. Due to lack of a main input, the grid-connected inverter should control the output voltage by supplying the power balance at a desired voltage [12].

From (19), the transfer function matrix of the converter can be obtained as follows:

$$G = C(sI - A)^{-1}B + D \tag{22}$$

where G is the system's transfer function, s is a variable in the Laplace domain of the operator, and I is an identity
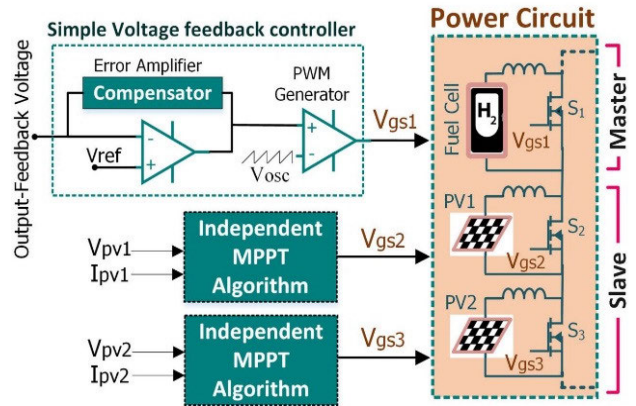

FIGURE 6. Overview of the control system for the SI-MISO converter [12].

matrix. The number of control variables is demonstrated by the G matrix's rank. The transfer function for the SI-MISO converter is expressed as follows [14]:

$$\text{For } n \text{ inputs}: \begin{bmatrix} y_1 \\ y_2 \\ \vdots \\ y_n \end{bmatrix} = \begin{bmatrix} g_{11} & g_{12} & \cdots & g_{n1} \\ g_{21} & g_{22} & \cdots & g_{n2} \\ \vdots & \vdots & \ddots & \cdots \\ g_{1n} & g_{2n} & \vdots & g_{nn} \end{bmatrix} \begin{bmatrix} u_1 \\ u_2 \\ \vdots \\ u_n \end{bmatrix}$$

$$\text{For } 2 \text{ inputs}: \begin{bmatrix} y_1 \\ y_2 \end{bmatrix} = \begin{bmatrix} g_{11} & g_{12} \\ g_{21} & g_{22} \end{bmatrix} \begin{bmatrix} u_1 \\ u_2 \end{bmatrix} \tag{23}$$

where the system's input vector is u, and its output vector is y. The transfer function between y_i and u_j is defined by g_{ij}. The control method consists of n independent controllers for each switch of the SI-MISO converter as a variable. Therefore, to control the converter with two inputs, the system has two independent control variables. The switch is linked to PV sources, which can be differentiated from the transfer function, responsible for the MPPT of this PV source. The other switches are responsible to control the output voltage.

In this paper, because we consider a two-port MISO converter with two output variables (V_C, I_L), the output voltage (V_C) generally cannot be controlled directly with linear controllers. Therefore, by using the inductor current (I_L) feedback in the PID cascade control structure, the output voltage

$$L\frac{d\hat{i}_L(t)}{dt} = \left(1 - \hat{d}_3(t)\right)\hat{v}_o(t) + \left(1 + \hat{d}_1(t) - \hat{d}_3(t)\right)\hat{v}_{pv}(t) + \left(-\hat{v}_o(t) - \hat{v}_{pv}(t) + V_{i_2}\right) + \hat{d}_1(t)\left(\hat{v}_{pv}(t) - V_{i_2}\right) \tag{18}$$

$$C_o\frac{d\hat{v}_o(t)}{dt} = \hat{i}_L(t)\left(1 - \hat{d}_3(t)\right) - \hat{i}_L(t)\hat{d}_3(t) - \frac{\hat{v}_o(t)}{R_o}, \quad C_{pv}\frac{dv_{pv}(t)}{dt} = \frac{\hat{v}_{pv}(t)}{R_{pv_{eq}}} + \hat{i}_L(t)\left(2\hat{d}_3(t) - 2\hat{d}_1(t) - 1\right) \tag{19}$$

$$A = \begin{bmatrix} 0 & \dfrac{1 + D_1 - D_3}{L} & \dfrac{1 - D_3}{L} \\ \dfrac{D_3 - D_1 - 1}{C_{in}} & \dfrac{1}{C_{in} \times R_{pv_{eq}}} & 0 \\ \dfrac{1 - D_3}{C_o} & 0 & \dfrac{-1}{R_o \times C_o} \end{bmatrix}; \quad B = \begin{bmatrix} \dfrac{V_{pv} - V_2}{L} & \dfrac{-V_o - V_{pv} + V_2}{L} \\ \dfrac{-I_L}{C_{in}} & \dfrac{I_L}{C_{in}} \\ 0 & \dfrac{-I_L}{C_o} \end{bmatrix};$$

$$C = \begin{bmatrix} 0 & 1 & 0 \end{bmatrix}; \quad D = 0 \tag{20}$$

(V_C) can be indirectly controlled. This method includes two PID controllers, as shown in Fig. 7.

Due to small signal characteristics of boost converters, the transfer function V_o/u is unstable and has a pole on the right side of the Root-Lucas diagram. A PID cascade controller can rectify this problem. As the first step, a PID controller is designed for the inductor current transfer function as follows:

$$T_s = \frac{I_L}{I_{ref}} = \frac{C_1(s) * H_1(s)}{1 + C_1(s) * H_1(s)} \tag{24}$$

where T_s, as shown in Fig. 8, is the transfer function of the inductor current, and its closed-loop equation is introduced in (19). H_1 is equal to I_L/u. The control system can be simplified once the first PID controller (C_1) is designed.
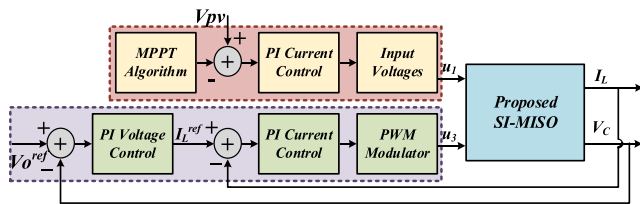
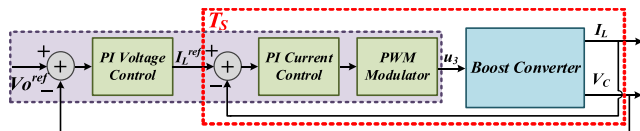**FIGURE 7.** The control diagram of the SI-MISO DC-DC converter.

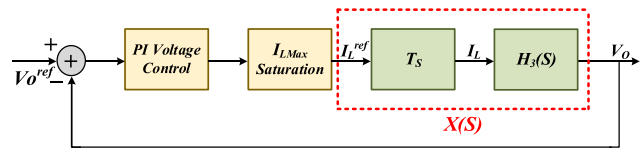**FIGURE 8.** The PID cascade structure.

FIGURE 9. First PID controller.

The output of T_s is then calculated using the inductor current. As a result, the transfer function $H_2(s)$ is proposed to design the second PID controller based on the output voltage reference in (26).

$$H_3(s) = \frac{V_C}{I_L} = H_2(s) * H_1(s)^{-1} \tag{25}$$

$$X(s) = \frac{V_C}{I_{L_{ref}}} = H_3(s) * T(s) \tag{26}$$

Eq. (26) indicates that $H_3(s)$ is related to the V_C/I_L equation, and the second PID controller is designed for the transfer function $X(s)$, as shown in Fig. 9.

When developing PID controllers, their dynamic responses must be considered. The dynamic response of the first loop related to the inductor current is considerably faster than the dynamics of the capacitor voltage [15], [18]. This difference between responses of two feedbacks cause unbalance

between two PID controllers. In each cycle, the inner loop, which consists of the inductor current feedback, has a faster transfer function compared to the external feedback, which consists of the output voltage feedback. Therefore, for an adequate design, the current loop's bandwidth must be ten times greater than the output voltage loop.

Parameter specifications of the PID controllers are given in Tables 1 and 2. Using the PID Tuner application in MATLAB and based on the trial-and-error method, the controller parameters can be obtained.

The phase margin of the converter should be within the range of [60°, 80°] [14], and the gain margin should be greater than 10 dB. Fig. 10 shows the Bode diagram of the converter before and after using the proposed PID cascade controller.

TABLE 1. The PID controller's parameters.

Controller	Value
PID$_1$	$K_{p_1} = 0.0073$
	$K_{i_1} = 14.9$
	$K_{d_1} = 1 \times 10^{-6}$
PID$_2$	$K_{p_2} = 0.0049$
	$K_{i_2} = 32.3$
	$K_{d_2} = 0$

TABLE 2. The PID controller's behaviors.

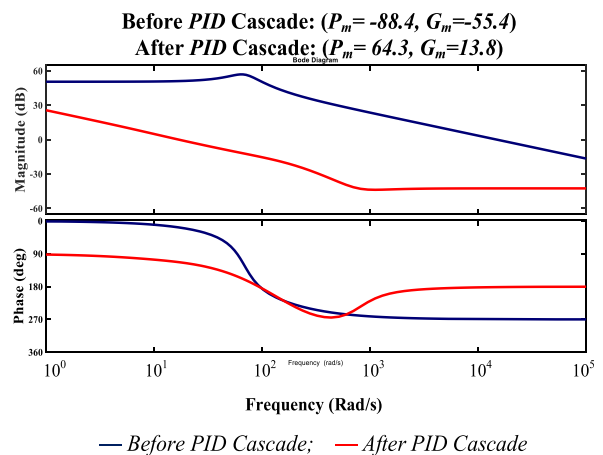|	PID$_1$	PID$_2$
Rise Time	0.0005 (s)	0.02 (s)
Settling Time	0.006 (s)	0.03 (s)
Overshoot	0.2%	0.9%
BW closed loop	4063 (rad/sec)	123 (rad/sec)

FIGURE 10. Bode plots of the closed loop system before and after the PID cascade controller.

IV. RESULTS

A. EXPERIMENTAL RESULTS

In this section, the proposed control method for the SI-MISO DC-DC converter is validated by experimental results

TABLE 3. Parameter specifications of the 100 W prototype converter.

| Parameters	Value
Switching frequency f_{sw}	10 kHz
Input voltage V_{in1} (Solar cell simulator)	~30V
Input voltage V_{in2} (Fuel cell simulator)	20V
Output Voltage V_o /Output power	100V/100W
Rated Output Current $I_{o_{full}}$	1A
Inductor current I_L	6A
Inductance L	1.2mH/28A max
Capacitances C_o and C_{in}	1000μF/450V
Switches S_1 and S_3	IXFH24N90P
Diodes D_2 and D_3	VS-65EPS12LHM3
Current sensors/ Voltage transducer	LA 55-P/ LV 25-P
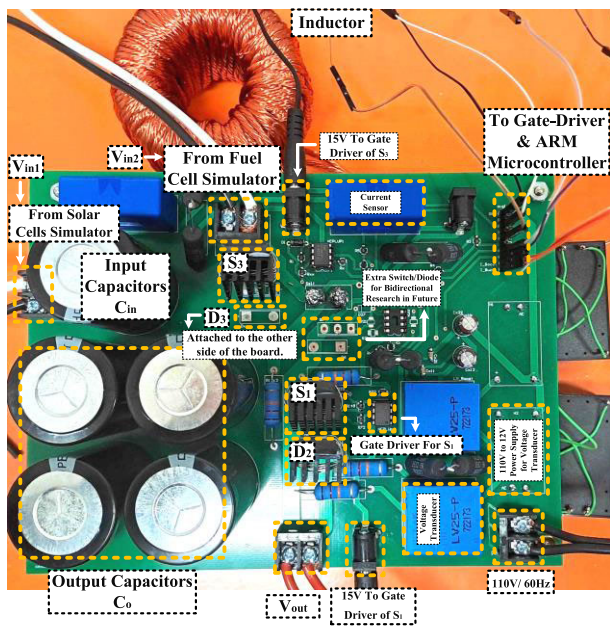
FIGURE 11. The prototype of the SI-MISO DC-DC converter with two inputs.

using a 100 W prototype converter. The parameters used for this prototype converter with two input sources to supply a stand-alone load are shown in Table 3. The prototype converter's system set-up for experiments in the lab is shown in Fig. 11. The converter can be used to manage power for solar PV panels or a battery storage system, and optimize energy utilization.

Figs. 12, 13 and 14 show experimental results with the input sources connected to solar cells and a fuel cell simulator. The output voltage, inductor current, and duty cycle of the switches S_1 and S_3 are shown in Fig. 12 during the open-loop operation under nominal conditions. The measured output voltage and inductor current are almost at 100 V and 6 A, respectively, close to their specifications in Table 3. The duty cycles of switches S_1 and S_3 are 0.36 and 0.75, respectively. These output voltage and inductor current are within the desired range, indicating that design parameters are selected correctly.

The system was further tested under closed-loop conditions, as shown in Figs. 13, 14, and 15. Firstly, the converter

was tested during a sudden disturbance of input sources. Fig. 13(a) shows changes in the fuel cell voltage, V_{FC}, from 20 V to 12 V; Figs. 13(b) and 13(c) show changes in the PV cell's voltage from 30 V to 12 V, and V_{FC} from 20 V to 15 V, separately and simultaneously.

Secondly, the converter was also tested for a sudden load change. In Fig. 14(a), the load was suddenly reduced from 100 Ω to 50 Ω, and in Fig. 14(b), the load was increased from 100 Ω to 200 Ω. The MPPT control for PV cells operates independently from the proposed PID cascade controller in the converter. Fig. 15 shows the results of the MPPT operation under a shading condition. It is found that the proposed system can successfully track the maximum power point despite the presence of shading. The MPPT algorithm can adjust the duty cycle of the converter to maintain the PV source at its maximum power point, while the PID cascade controller ensures that the system is operating at the highest efficiency.

The experimental results indicate that under challenging conditions, such as shading and sudden changes in input voltages and load, the proposed system maintains stable operation and an overall efficiency of 92.4% at full load. The components count is low in the converter, there are only two conducting switches/diodes in Stage two, and one conducting switch or diode in other two stages, leading to low conduction losses, and contributing to a high system efficiency. In terms of the control system performance, the proposed controller has fast dynamic response, zero steady-state errors, and high stability under various testing scenarios; and it also has a low cost and is simple to implement.

B. ANALYSIS OF POWER LOSS AND COMPARISON WITH PREVIOUS WORKS

The power transfer efficiency is defined as the ratio of the power flowing out of the converter to the power flowing into the converter from all input sources (both the PV source and the fuel cell). To determine the power losses of the components, we can calculate the root mean square (RMS) current in (27) and the equivalent resistance of each component.

$$I_{s(rms)} = \sqrt{\frac{1}{Ts} \int (I_s + \Delta I_s)^2 dt} \tag{27}$$

Table 4 shows the percentage of power losses for each component. The inductor has the highest power losses, as it is the only component with the current flowing through it at all stages. Fig. 16 shows the overall efficiency of the converter under different output power through experiments.

Table 5 shows the comparison between the converter in this paper and multi-input converters in [6], [12], [21], [22], [23], [24], [25], [26], [27], [28], and [29]. Due to their low output voltage levels, converters in [21], [23], [24], [25], and [27] are not effective to connect renewable energy sources to power grids. The converter in this paper has the fewest elements count, and thus, can be realized with a smaller volume and a lower price. In terms of the control method, in the converter in this paper, each switch is controlled separately without

TABLE 4. RMS current and power losses of each component.

Components	RMS current	Element resistance	Power losses	Percentage of losses
Switch S_1	$I_{S_1(rms)} = (\sqrt{D_1} \times I_{i_1})/(D_1 + D_2)$	$r_{DS_{on}} = 40$ mΩ	1.685 W	25.22%
Switch S_3	$I_{S_3(rms)} = I_{i_1}/\sqrt{D_3}$	$r_{DS_{on}} = 40$ mΩ	1.265 W	18.93%
Diode D_2	$I_{D_2(rms)} = I_o/\sqrt{D_2}$	$r_D = 3.98$ mΩ, $V_{FD} = 0.74$ V	0.706 W	10.58%
Diode D_3	$I_{D_3(rms)} = I_{i_1}/\sqrt{D_3}$	$r_D = 3.98$ mΩ, $V_{FD} = 0.74$ V	0.551 W	8.24%
C_o	$I_{C_o(rms)} = I_{o_1}/\sqrt{(1-D_2)/D_2}$	$r_C = 20$ mΩ	0.137 W	2.05%
C_{in}	$I_{C_o(rms)} = I_{i_1}/\sqrt{(1-D_3)/D_3}$	$r_C = 20$ mΩ	0.113 W	1.7%
L	$I_{L(rms)} = I_o/D_2$	$r_L = 40$ mΩ	2.224 W	33.28%

TABLE 5. Comparison of the studied converter in this paper and existing multi-input converters with two input sources in the literature.

|	[21]	[22]	[23]	[24]	[25]	[26]	[27]	[28]	[29]	[6]	[12]	This paper
Power output [W]	236	-	200	100	100	100	450	100	96	1000	300	100
Independent control of power and voltage	×	×	×	×	×	×	×	×	×	×	✓	✓
Independent power transmission	✓	×	✓	×	×	×	✓	✓	×	✓	✓	✓
Extendable	✓	✓	✓	✓	✓	×	✓	✓	✓	✓	✓	✓
Output voltage levels	Low	High	Low	Low	Low	High	Low	High	Low	High	High	High
Max. voltage across switches	High	High	High	High	High	High	Low	Low	Low	Low	Low	Low
Inductors	1	3	1	1	2	2	3	4	2	2	3	1
Switches	3	3	3	3	2	2	3	2	2	2	2	2
Diodes	3	3	3	3	3	2	1	6	2	3	3	2
Capacitors	1	3	2	1	1	2	2	2	2	4	4	2
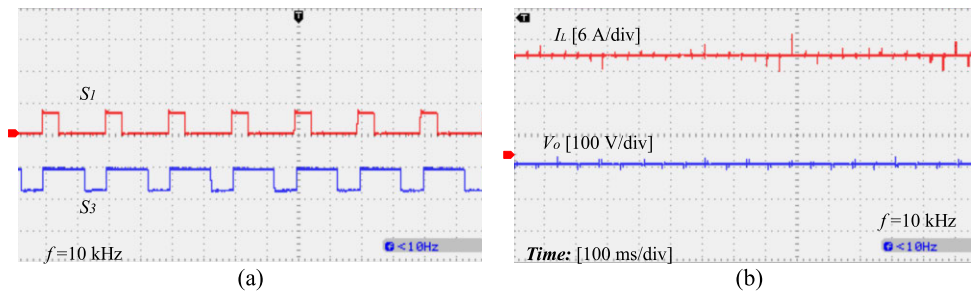
FIGURE 12. Experimental waveforms of the converter in open-loop operation: (a) duty cycle of switches S_1 and S_3, (b) open-loop operation under nominal conditions.
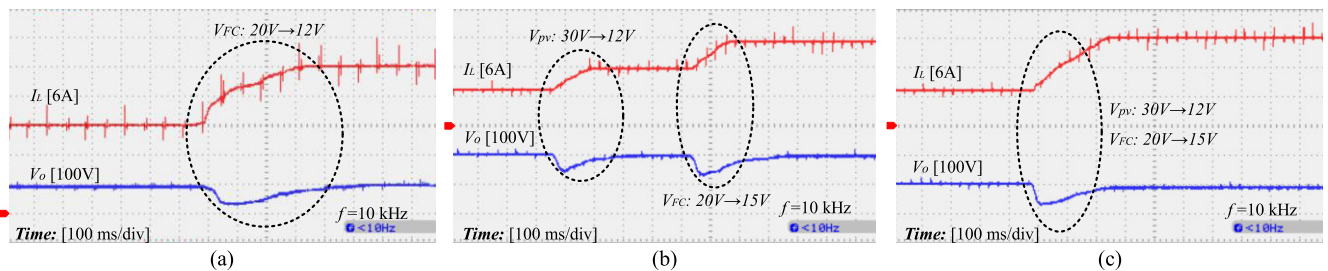

FIGURE 13. Experimental waveforms of the output voltage (V_O) and inductor current (I_L) of the converter: (a) change the fuel cell voltage V_{FC} form 20 V to 12 V; (b) change PV cell voltage V_{pv} from 30 V to 12 V, and V_{FC} from 20 V to 15 V at two different time separately; and (c) change V_{pv} from 30 V to 12 V and V_{FC} from 20 V to 15 V simultaneously.

using a decoupling network, so the control can be done in a straightforward and practical way and is much simpler in experimental implementation than other multi-variable converters.
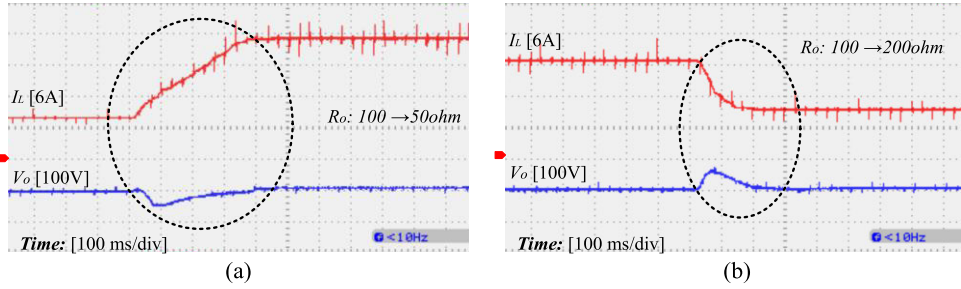
FIGURE 14. Experimental waveforms of the output voltage (V_o) and inductor current (I_L) of the converter: (a) the load decreased from 100 Ω to 50 Ω; (b) the load increased from 100 Ω to 200 Ω.
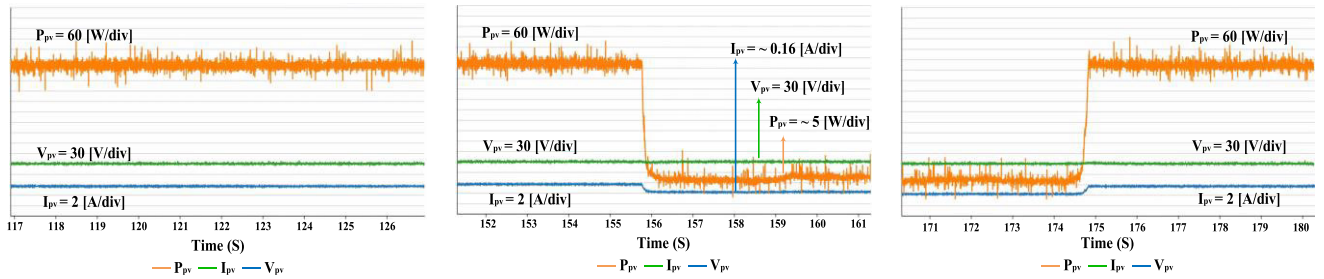

FIGURE 15. Testing the MPPT controller for the PV source in the converter under a shading condition.

TABLE 6. The simulated start-up behaviors of the proposed PID cascade controller.

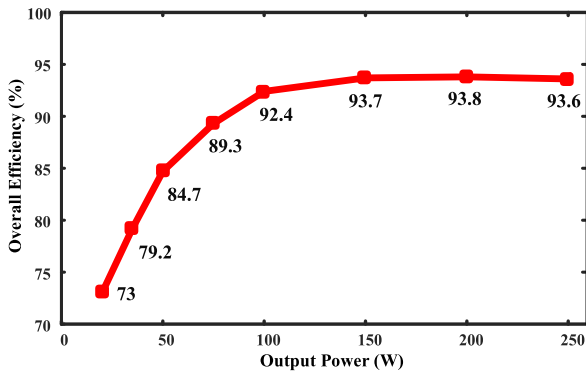|	PID Cascade controller with a MPPT
Rise Time	0.0108 (Seconds)
Settling Time	0.0473 (Seconds)
Overshoot	0%

FIGURE 16. The total efficiency of the converter under different output power through experiments.

FIGURE 17. The simulated start-up responses of the inductor current (top) and the output voltage (bottom) of the converter under normal operation (S- seconds).

Fig. 17 shows the simulated start-up responses of the inductor current and the output voltage of the converter by MATLAB/Simulink. Table 6 shows the simulated rise time, settling time and overshoot during the start-up.

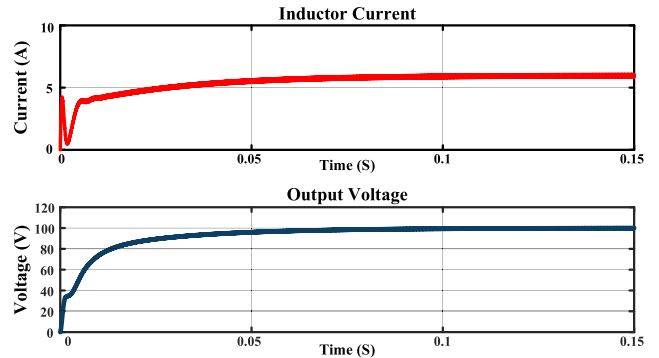To improve the converter's efficiency, as the future work, soft-switching techniques can be applied to the circuit; the wide-bandgap (WBG) semiconductors, such as GaN, can be used to reduce the forward resistance in switches and diodes; and a better inductor can be designed to reduce power losses.

V. CONCLUSION

In this paper, a non-isolated single-inductor multi-input single-output DC-DC boost converter with multiple power sources is investigated, and a novel PID cascade controller is proposed to indirectly control the output voltage of the converter with the inductor current. Since this converter can control the output voltage and the input power independently, the MPPT can be used for each PV source, regardless of the control scheme for the output voltage. The proposed controller is validated using a 100-W prototype converter with two input sources. It is found that the controller maintains a fast dynamic response, zero steady-state errors, and is highly

robust against disturbances. This converter benefits from a simple structure with fewer components compared to other multi-input converters in the literature and thus achieved 92.4% efficiency in the prototype.

REFERENCES

[1] F. Nejabatkhah, S. Danyali, S. H. Hosseini, M. Sabahi, and S. M. Niapour, "Modeling and control of a new three-input DC–DC boost converter for hybrid PV/FC/battery power system," *IEEE Trans. Power Electron.*, vol. 27, no. 5, pp. 2309–2324, May 2012.

[2] P. Yang, C. K. Tse, J. Xu, and G. Zhou, "Synthesis and analysis of double-input single-output DC/DC converters," *IEEE Trans. Ind. Electron.*, vol. 62, no. 10, pp. 6284–6295, Oct. 2015.

[3] X. L. Li, Z. Dong, C. K. Tse, and D. D. Lu, "Single-inductor multi-input multi-output DC–DC converter with high flexibility and simple control," *IEEE Trans. Power Electron.*, vol. 35, no. 12, pp. 13104–13114, Dec. 2020.

[4] Y.-M. Chen, Y.-C. Liu, and S.-H. Lin, "Double-input PWM DC/DC converter for high-/low-voltage sources," *IEEE Trans. Ind. Electron.*, vol. 53, no. 5, pp. 1538–1545, Oct. 2006.

[5] H. Wu, K. Sun, S. Ding, and Y. Xing, "Topology derivation of nonisolated three-port DC–DC converters from DIC and DOC," *IEEE Trans. Power Electron.*, vol. 28, no. 7, pp. 3297–3307, Jul. 2013.

[6] P. Mohseni, S. H. Hosseini, M. Sabahi, T. Jalilzadeh, and M. Maalandish, "A new high step-up multi-input multi-output DC–DC converter," *IEEE Trans. Ind. Electron.*, vol. 66, no. 7, pp. 5197–5208, Jul. 2019.

[7] G. Chen, Y. Liu, X. Qing, M. Ma, and Z. Lin, "Principle and topology derivation of single-inductor multi-input multi-output DC–DC converters," *IEEE Trans. Ind. Electron.*, vol. 68, no. 1, pp. 25–36, Jan. 2021.

[8] M. S. Mahdavi, M. Karimzadeh, T. Rahimi, and G. B. Gharehpetian, "A fault-tolerant bidirectional converter for battery energy storage systems in DC microgrid," *Electronics*, vol. 12, no. 3, p. 679, 2023.

[9] M. Azizi, M. Mohamadian, and R. Beiranvand, "A new family of multi-input converters based on three switches leg," *IEEE Trans. Ind. Electron.*, vol. 63, no. 11, pp. 6812–6822, Nov. 2016.

[10] S. Dusmez, X. Li, and B. Akin, "A new multiinput three-level DC/DC converter," *IEEE Trans. Power Electron.*, vol. 31, no. 2, pp. 1230–1240, Feb. 2016.

[11] F. Liu, Z. Wang, Y. Mao, and X. Ruan, "Asymmetrical half-bridge double-input DC/DC converters adopting pulsating voltage source cells for low power applications," *IEEE Trans. Power Electron.*, vol. 29, no. 9, pp. 4741–4751, Sep. 2014.

[12] E. Amiri, R. R. Khorasani, E. Adib, and A. Khoshkbar-Sadigh, "Multi-input high step-up DC–DC converter with independent control of voltage and power for hybrid renewable energy systems," *IEEE Trans. Ind. Electron.*, vol. 68, no. 12, pp. 12079–12087, Dec. 2021.

[13] J. Ruan, F. Liu, X. Ruan, D. Yang, Y. Li, and K. Jin, "Isolated multiple-input DC/DC converter using alternative pulsating source as building cells," in *Proc. Int. Power Electron. Conf.*, Sapporo, Japan, Jun. 2010, pp. 1463–1470.

[14] A. Asadi, K. Abbaszadeh, and A. Darabi, "Modeling and control of a single-inductor multi-input multi-output DC–DC boost converter for PV applications," in *Proc. 13th Power Electron., Drive Syst., Technol. Conf. (PEDSTC)*, Tehran, Iran, Feb. 2022, pp. 51–55.

[15] M. Salimi, F. Radmand, and M. H. Firouz, "Dynamic modeling and closed-loop control of hybrid grid-connected renewable energy system with multi-input multi-output controller," *J. Modern Power Syst. Clean Energy*, vol. 9, no. 1, pp. 94–103, Jan. 2021.

[16] B. Wang, L. Xian, V. R. K. Kanamarlapudi, K. J. Tseng, A. Ukil, and H. B. Gooi, "A digital method of power-sharing and cross-regulation suppression for single-inductor multiple-input multiple-output DC–DC converter," *IEEE Trans. Ind. Electron.*, vol. 64, no. 4, pp. 2836–2847, Apr. 2017.

[17] S. Danyali, S. H. Hosseini, and G. B. Gharehpetian, "New extendable single-stage multi-input DC/DC/AC boost converter," *IEEE Trans. Power Electron.*, vol. 29, no. 2, pp. 775–788, Feb. 2014.

[18] R. Vilanova and O. Arrieta, "PID tuning for cascade control system design," in *Proc. Can. Conf. Electr. Comput. Eng.*, May 2008, pp. 001775–001778.

[19] Z. J. Geng and L. S. Haynes, "Six degree-of-freedom active vibration control using the stewart platforms," *IEEE Trans. Control Syst. Technol.*, vol. 2, no. 1, pp. 45–53, Mar. 1994.

[20] A. Hosseini, A. S. Badeli, M. Davari, S. Sheikhaei, and G. B. Gharehpetian, "A novel, software-defined control method using sparsely activated micro-controller for low-power, multiple-input, single-inductor, multiple-output DC–DC converters to increase efficiency," *IEEE Trans. Ind. Electron.*, vol. 70, no. 3, pp. 2959–2970, Mar. 2023.

[21] A. Nahavandi, M. T. Hagh, M. B. B. Sharifian, and S. Danyali, "A non-isolated multiinput multioutput DC–DC boost converter for electric vehicle applications," *IEEE Trans. Power Electron.*, vol. 30, no. 4, pp. 1818–1835, Apr. 2015.

[22] Y. Tong, Z. Shan, J. Jatskevich, and A. Davoudi, "A nonisolated multiple-input multiple-output DC–DC converter for DC distribution of future energy efficient homes," in *Proc. 40th Annu. Conf. IEEE Ind. Electron. Soc.*, Dallas, TX, USA, Oct. 2014, pp. 4126–4132.

[23] H. Keyhani and H. A. Toliyat, "A ZVS single-inductor multi-input multi-output DC–DC converter with the step up/down capability," in *Proc. IEEE Energy Convers. Congr. Expo.*, Denver, CO, USA, Sep. 2013, pp. 5546–5552.

[24] H. Behjati and A. Davoudi, "A multiple-input multiple-output DC–DC converter," *IEEE Trans. Ind. Appl.*, vol. 49, no. 3, pp. 1464–1479, May 2013.

[25] M. Jafari, G. Hunter, and J. Guo Zhu, "A new topology of multi-input multi-output buck-boost DC–DC converter for microgrid applications," in *Proc. IEEE Int. Conf. Power Energy (PECon)*, Kota Kinabalu, Malaysia, Dec. 2012, pp. 286–291.

[26] M. R. Banaei, H. Ardi, R. Alizadeh, and A. Farakhor, "Non-isolated multi-input-single-output DC/DC converter for photovoltaic power generation systems," *IET Power Electron.*, vol. 7, no. 11, pp. 2806–2816, 2014.

[27] R.-J. Wai, C.-Y. Lin, J.-J. Liaw, and Y.-R. Chang, "Newly designed ZVS multi-input converter," *IEEE Trans. Ind. Electron.*, vol. 58, no. 2, pp. 555–566, Feb. 2011.

[28] J. Zeng, W. Qiao, and L. Qu, "An isolated multiport DC–DC converter for simultaneous power management of multiple renewable energy sources," in *Proc. IEEE Energy Convers. Congr. Expo. (ECCE)*, Raleigh, NC, USA, Sep. 2012, pp. 3741–3748.

[29] L.-W. Zhou, B.-X. Zhu, and Q.-M. Luo, "High step-up converter with capacity of multiple input," *IET Power Electron.*, vol. 5, no. 5, pp. 524–531, 2012.

[30] R. W. Erickson and D. Maksimovic, *Fundamentals of Power Electronics*, 2nd Ed. New York, NY, USA: Kluwer Academic, 2000.

[31] K. Warwick and D. Rees, *Industrial Digital Control Systems* (IEE Control Engineering Series 37). Stevenage, U.K: Pereginus, 1988.

ALIREZA ASADI was born in Kerman, Iran, in 1998. He received the B.S. degree in electrical engineering from the K. N. Toosi University of Technology, Tehran, in 2021. He is currently pursuing the M.Sc. degree in electrical engineering with the University of Saskatchewan, Saskatoon, SK, Canada. His research interests include multi-port and high-gain dc–dc converters, power electronics applications and renewable energy systems, resonant converters, and microgrids.

MOHAMMAD SALEH KARIMZADEH was born in Kerman, Iran. He received the B.S. degree in electrical engineering from the K. N. Toosi University of Technology, Tehran, Iran, in 2021. He is currently pursuing the M.Sc. degree in electrical engineering with the Amirkabir University of Technology, Tehran. His research interests include multi-port and high gain dc–dc converters, power electronics applications and renewable energy systems, resonant converters, battery energy storage, and microgrids.

XIAODONG LIANG (Senior Member, IEEE) was born in Lingyuan, Liaoning, China. She received the B.Eng. and M.Eng. degrees in electrical engineering from Shenyang Polytechnic University, Shenyang, China, in 1992 and 1995, respectively, the M.Sc. degree in electrical engineering from the University of Saskatchewan, Saskatoon, Canada, in 2004, and the Ph.D. degree in electrical engineering from the University of Alberta, Edmonton, Canada, in 2013.

From 1995 to 1999, she was a Lecturer with Northeastern University, Shenyang, China. In October 2001, she joined Schlumberger (SLB), Edmonton, Canada, and was promoted to Principal Power Systems Engineer with this world's leading oil field service company in 2009. She was with Schlumberger for almost 12 years, until August 2013. From 2013 to 2019, she was with Washington State University, Vancouver, WA, USA, and the Memorial University of Newfoundland, St. John's, NL, Canada, as an Assistant Professor, and later an Associate Professor. In July 2019, she joined the University of Saskatchewan, Saskatoon, where she is currently a Professor and the Canada Research Chair in Technology Solutions for Energy Security in Remote, Northern, and Indigenous Communities. She was an Adjunct Professor with the Memorial University of Newfoundland, from 2019 to 2022. Her research interests include power systems, renewable energy, and electric machines.

Dr. Liang is a registered Professional Engineer in the Province of Saskatchewan, Canada, a fellow of IET, and the Deputy Editor-in-Chief of IEEE TRANSACTIONS ON INDUSTRY APPLICATIONS.
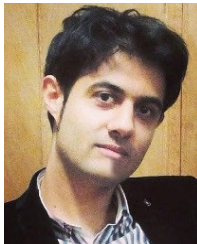
MOHAMMAD SAEED MAHDAVI was born in Isfahan, Iran, in 1990. He received the B.Sc. degree from the Isfahan University of Technology, Isfahan, in 2012, and the M.Sc. and Ph.D. degrees from the Amirkabir University of Technology (AUT), Tehran, Iran, in 2014 and 2019, respectively. He is currently a Postdoctoral Researcher with AUT. From 2014 to 2022, he was the Technical Manager of AUT Microgrid Project as one of the sub-projects of the Iran Grand (National) Smart Grid Project under the supervision of Prof. G. B. Gharehpetian. His current research interests include power electronics, microgrids, electric drives, energy storage systems, DG, and smart grids. He is the Winner of three national prizes, the Best Dissertation Award, from the Power Electronics Society of Iran (PESI), in February 2020, the Iranian Scientific Organization of Smart Grids (ISOSG), in December 2020, and AUT, in December 2020, for the Ph.D. dissertation.

GEVORK B. GHAREHPETIAN (Senior Member, IEEE) received the Ph.D. degree (Hons.) in electrical engineering from Tehran University, Tehran, Iran, in 1996.

He was with the High Voltage Institute, RWTH Aachen, Aachen, Germany. He was also an Assistant Professor, from 1997 to 2003, an Associate Professor, from 2004 to 2007, and has been a Professor, since 2007, with the Amirkabir University of Technology (AUT). He is the author of more than 1400 journal and conference papers. His teaching and research interests include smart grids, microgrids, FACTS and HVdc systems, and monitoring of power transformers and its transients.

Prof. Gharehpetian is a Distinguished Member of CIGRE and IAEEE. He was selected by the Ministry of Science Research and Technology (MSRT) as a Distinguished Professor of Iran, by the Iranian Association of Electrical and Electronics Engineers (IAEEE) as a Distinguished Researcher of Iran, by the Iran Energy Association (IEA) as the Best Researcher of Iran in the field of energy, by the MSRT as a Distinguished Researcher of Iran, by the Academy of Science of the Islamic Republic of Iran as a Distinguished Professor of electrical engineering, by the National Elites Foundation as a Laureates of Alameh Tabatabaei Award, and was awarded the National Prize in 2008, 2010, 2018, 2018, 2019, and 2019, respectively. As a Ph.D. Student, he has received scholarship from the German Academic Exchange Service (DAAD), from 1993 to 1996. Since 2004, he has been the Editor-in-Chief of the *Journal of Iranian Association of Electrical and Electronics Engineers*. Based on the Web of Science database (2005–2022), he is among the world's top 1% elite scientists according to Essential Science Indicators (ESI) ranking system.

• • •